



PERGAMON

Journal of the Mechanics and Physics of Solids
50 (2002) 695–716

JOURNAL OF THE
MECHANICS AND
PHYSICS OF SOLIDS

www.elsevier.com/locate/jmps

Self-consistent elastoplastic stress solutions for functionally graded material systems subjected to thermal transients

S. Pitakthapanaphong, E.P. Busso*

*Department of Mechanical Engineering, Imperial College of Science, Technology and Medicine,
Exhibition Road, London SW7 2BX, UK*

Received 11 April 2001; received in revised form 23 July 2001

Abstract

In this work, a self-consistent constitutive framework is proposed to describe the behaviour of a generic three-layered system containing a functionally graded material (FGM) layer subjected to thermal loading. Analytical and semi-analytical solutions are obtained to describe the thermo-elastic and thermo-elastoplastic behaviour of a three-layered system consisting of a metallic and a ceramic layer joined together by an FGM layer of arbitrary composition profile. Solutions for the stress distributions in a generic FGM system subjected to arbitrary temperature transient conditions are presented. The homogenisation of the local elastoplastic FGM behaviour in terms of the properties of its individual phases is performed using a self-consistent approach. In this work, power-law strain hardening behaviour is assumed for the FGM metallic phase. The stress distributions within the FGM systems are compared with accurate numerical solutions obtained from finite element analyses and good agreement is found throughout. Solutions are also given for the critical temperature transients required for the onset of plastic deformation within the three-layered systems. © 2002 Elsevier Science Ltd. All rights reserved.

Keywords: Functionally graded materials; Self-consistent; Homogenisation; Constitutive formulations

1. Introduction

In a large number of engineering applications, individual components are exposed to local loading conditions which can vary greatly with location. In such cases, the

* Corresponding author. Tel.: +44-0171-594-7084; fax: +44-0171-823-8845.
E-mail address: e.busso@ic.ac.uk (E.P. Busso).

use of dissimilar materials, such as metals and ceramics, may be required. However, the abrupt transitions in microstructure and composition between the different materials often result in high residual stress regions and local stress concentrations which can lead to the subsequent nucleation of microcracks at or near the bimaterial interface. The intensity and extent of the stress concentration effects due to the large mismatch in properties can be substantially reduced if the microstructure is gradually changed from that of the metal to that of the ceramic. A relatively new class of materials known as functionally graded materials (FGMs) has recently been developed to minimise such property mismatch effects.

The composition and microstructure of an FGM varies with location, resulting in spatially dependent properties. The composition profile can take different forms depending on the required performance. Within an FGM, the different material phases have different functions. For example, in a metal–ceramic FGM, the metal-rich side is typically placed in regions where mechanical properties, such as toughness, need to be high. In contrast, the ceramic-rich side, which has lower thermal conductivity and can withstand high temperatures, is placed in regions where there are potentially sharp temperature gradients.

The real advantages of using an FGM as an alternative to two dissimilar materials joined directly together include: smoothing of thermal stress distributions across the layers (Choules and Kokini, 1996; Wetherhold et al., 1996), minimisation or elimination of stress concentrations and singularities at free edges (Lee and Erdogan, 1994/1995; Yang and Munz, 1997), increase in the bimaterial bonding strength (Howard et al., 1994a, b), and improved fracture toughness compared to that of monolithic ceramics as a result of the plastic deformation of the metallic phase (Erdogan, 1995; Jin and Batra, 1996; Shaw, 1998). Typical applications of FGMs are in high temperature coatings for combustion chambers and airfoils in the aerospace and power generation industries, coatings in microelectronics and optoelectronics applications, orthopaedic implants and wear-resistant coatings in bearings, gears, cams and machine tools (Miyamoto, 1996).

Analytical and numerical studies have been carried out to investigate the thermo-mechanical behaviour of FGMs (e.g. Freund, 1993; Giannakopoulos et al., 1995; Finot and Suresh, 1996; Dao et al., 1997; Weissenbek et al., 1997). The results of a microscopic study, where the anisotropic properties of each individual metallic grain in the FGM are described using crystal plasticity, have been reported in Dao et al. (1997). Only limited amount of analytical work describing the thermo-elastic behaviour of FGMs have been reported to date and most of it has been limited to FGMs with linear compositional gradations. This includes the work of Freund (1993), where solutions for the stress distributions in graded semiconductor layers were derived using linear elastic plate theory. The resulting expressions for the in-plane strains and curvatures were later applied to a Ni–Al₂O₃ system by Giannakopoulos et al. (1995). Since the thermo-mechanical behaviour of an FGM strongly depends on its composition profile, which in many instances is far from linear due to feasibility in manufacturing, the ability to understand and predict the behaviour of an FGM system with a generic composition profile is of prime importance. Accurate FGM constitutive models can, in turn, be used as a design tool for FGM manufacturing so that the optimal profile is tailored to suit a specific application.

In a metal–ceramic FGM, yielding in the metallic phase can greatly affect the stress distribution within the FGM and thus a stress analysis based only on elastic material behaviour will not be accurate. A similar issue applies to metal matrix composites (e.g. see Olsson et al., 1995). In such cases, it is worth noting that plastic deformation can occur solely as a result of thermal loads. Numerical investigations have also been carried out to study the thermo-elastoplastic behaviour of metal–ceramic FGMs using finite element (FE) techniques (Giannakopoulos et al., 1995; Finot and Suresh, 1996; Weissenbek et al., 1997). However, no analytical or semi-analytical solutions have been reported till date. Finite element analyses, although accurate, involve extensive and costly computations. Therefore there is a strong need for accurate analytical formulations to predict nonlinear FGM behaviour.

The homogenisation of the local FGM material behaviour can be performed using a self-consistent scheme. In the classical self-consistent approach, (e.g. see Kroner, 1961; Budiansky and Wu, 1962), the interaction of a single grain, or inclusion, with the surrounding polycrystalline material is approximated by a spherical inclusion embedded in a homogeneous polycrystalline matrix with the same elastic property as the inclusion. For an elasto-plastic material, the term ‘self-consistent’ implies that the microscopic stresses and strains satisfy equilibrium and compatibility at the grain/phase boundaries, and that the average stress and strain over all the grains must yield the corresponding macroscopic values. Eshelby’s solutions (Eshelby, 1957) are relied upon to link the macroscopic stresses (or stress rates, $\dot{\sigma}_{ij}^*$) with the microscopic or average stresses (or stress rates, $\dot{\sigma}_{ij}$) in each grain (Kroner, 1961; Budiansky and Wu, 1962),

$$\dot{\sigma}_{ij} = \dot{\sigma}_{ij}^* + 2\mu^*(1 - \beta)(\dot{\epsilon}_{ij}^{*p} - \dot{\epsilon}_{ij}^p), \quad \text{for } i, j = 1, 2, 3. \quad (1)$$

Here, μ^* is the polycrystal aggregate shear modulus, β Eshelby’s elastic accommodation factor (Eshelby, 1957), and $\dot{\epsilon}_{ij}^p$ and $\dot{\epsilon}_{ij}^{*p}$ are the microscopic and macroscopic plastic strain rates, respectively.

In Eq. (1), an elastic interaction between the grain and the polycrystal aggregate is implicitly assumed, thus a high constraint is imposed on the inclusion by the surrounding elastic aggregate. In reality, such high constraint is partially relaxed by the plastic deformation of the polycrystalline aggregate. The work of Berveiller and Zaoui (1979) addressed this problem by introducing an additional plastic accommodation factor into Eq. (1). In more recent work, Cailletaud and Pilvin (1995) and Busso (1999) (see also Busso et al., 2001a, b) described the behaviour of multiphase materials using tensorial interphase accommodation variables, which enable accurate uniaxial self-consistent predictions to be obtained for inclusion volume fractions above which self-consistent predictions cease to be accurate (e.g. > 30%).

An alternative homogenisation method to the classical self-consistent approach is that derived from a variational procedure. The early work of Hashin and Shtrikman (1963) introduced a variational procedure to estimate the effective modulus of elastic composites with statistically isotropic microstructures. This approach allowed rigorous upper and lower bounds to be obtained for the effective modulus tensor of the composite. A generalisation of Hashin–Shtrikman’s bounds for nonlinear composites was presented by Talbot and Willis (1985), and an alternative variational formulation was later on proposed by Ponte Castañeda (1991). The latter relies on the effective modulus

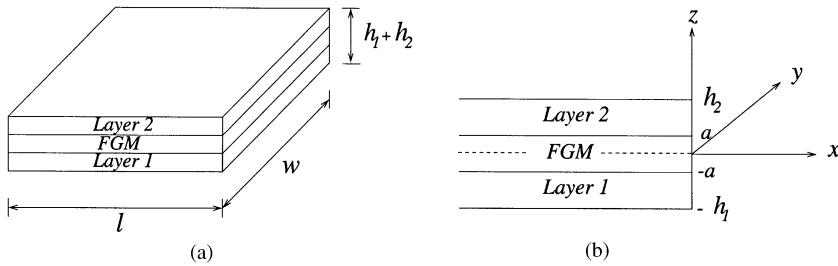


Fig. 1. Schematic representation of (a) a three-layered model, and (b) coordinate axes and dimensions of the three-layered system.

tensor of ‘linear elastic comparison composites’, whereby the effective stress potentials of nonlinear composites are expressed in terms of the corresponding potentials for linear composites with similar microstructural distributions, to generate the corresponding bounds. Ponte Castañeda’s variational principles (1991) have also been used to derive elastoplastic relations for metal matrix composites reinforced by spheroidal elastic particles (Li and Ponte Castañeda, 1994). The latter formulation will be applied to an FGM system to provide a basis with which predictions obtained with the homogenisation formulation to be proposed here can be compared to.

In this work, the analytical thermo-elastic framework proposed by Freund (1993) is first generalised to include various forms of nonlinear FGM compositional gradations. This is then followed by the description of the elastoplastic behaviour of a generic FGM using a self-consistent constitutive approach (Cailletaud and Pilvin, 1995; Busso, 1999). The metallic phase within the FGM will be considered to be a generic power-law strain hardening material. The calibration of the self-consistent formulation using embedded unit cell FE techniques is next described, and the results compared with the variational solutions of Li and Ponte Castañeda (1994). The self-consistent solutions for the stress distributions within the three-layered FGM system are then compared with accurate FE solutions. Finally, the critical temperature transients required for the onset of plastic deformation within the three-layered systems are given, together with a comparison between the magnitudes of elastic and elastoplastic curvatures.

2. Thermo-elastic analysis under an arbitrary temperature transient

2.1. Analytical formulation for a generic FGM composition profile

Consider a three-layered system made up of a compositionally graded layer in between two homogeneous materials, as shown in Fig. 1, subjected to a uniform temperature which may vary with respect to time.

Let the total length, width and height of the multilayer system be given by l , w and $(h_1 + h_2)$, respectively, see Fig. 1(a). When $l \gg (h_1 + h_2) \gg w$, the geometry of the model allows it to be idealised as a plane stress beam, and the variables of interest depend only on the out-of-plane coordinate, z . Furthermore, a multi-layer system with

$l = w \gg (h_1 + h_2)$, corresponds to a system under equal in-plane or biaxial stresses, herefrom to be referred to as the biaxial stress model. The in-plane geometry of the layered structure is shown in Fig. 1(b). The FGM layer extends from $z = -a$ to $z = +a$ and, for continuous property assumptions to be valid, the thickness of this layer must be significantly larger than its dominant microstructural length scale (e.g. grain size). The interfaces between the different layers are assumed to be perfectly bonded at all times and the multilayer system behaviour to be linear elastic. Moreover, the material is assumed to be initially stress free.

By assuming small strain kinematics, the total strain, $\tilde{\varepsilon}^*$, applied in the plane of the multilayer system, (where $\tilde{\varepsilon}^* = \varepsilon_{xx}^*$ for the plane stress case and $\tilde{\varepsilon}^* = \varepsilon_{xx}^* = \varepsilon_{yy}^*$ for the equal biaxial stress case), can be decomposed into an elastic, $\tilde{\varepsilon}^{*e}$, and a thermal, $\tilde{\varepsilon}^{*th}$, component as

$$\tilde{\varepsilon}^* = \tilde{\varepsilon}^{*e} + \tilde{\varepsilon}^{*th}. \quad (2)$$

When the total strain $\tilde{\varepsilon}^*$ is considered to be a function of the out-of-plane coordinate, z , it can be shown that the small-strain compatibility equations lead to a linear relation between the total strain and curvature, κ ,

$$\tilde{\varepsilon}^*(z) = \varepsilon_0 + \kappa z, \quad (3)$$

where ε_0 is the strain at the mid-plane of the FGM layer ($z = 0$).

Under plane stress conditions, the only non-zero stress component, $\tilde{\sigma}^*(z)$, is given by

$$\tilde{\sigma}^*(z) = E^*(z) [\tilde{\varepsilon}^*(z) - \alpha^*(z) \Delta T]. \quad (4)$$

Here, $\Delta T = T - T_0$, where T_0 is the stress-free temperature and T the homogeneous temperature in the multilayer system. For equal biaxial stress conditions,

$$\sigma_{xx}^* = \sigma_{yy}^* = \tilde{\sigma}^*(z). \quad (5)$$

Substitution of Eq. (3) into Eq. (4) gives

$$\tilde{\sigma}^*(z) = E^*(z) [\varepsilon_0 + \kappa z - \alpha^*(z) \Delta T]. \quad (6)$$

Expressions for ε_0 and κ (given in Freund, 1993), can be derived on the basis that the resultant force and moment arising from the stress distribution through the thickness, i.e. along the z -axis, must equilibrate any applied in-plane force and bending moment, respectively.

Let the volume fraction of the layer 2 material within the FGM vary as a function of the coordinate, z , and be arbitrarily defined by a generic function, $\hat{V}(z)$, which satisfies the following conditions at the homogeneous layers' interfaces,

$$\hat{V}(z) = \begin{cases} 0 & \text{at } z = -a, \\ 1 & \text{at } z = a. \end{cases} \quad (7)$$

The elastic properties of the FGM, given by its Young's modulus, E^* , and Poisson's ratio, ν^* , together with the coefficient of thermal expansion, α^* , are assumed to vary

Table 1
Thermo-elastic properties for the metallic (Ni) and ceramic (Al_2O_3)
phases (Giannakopoulos et al., 1995)

Material	E (GPa)	ν	α ($^\circ\text{C}^{-1}$)
Al_2O_3	380	0.25	7.4×10^{-6}
Ni	214	0.31	15.4×10^{-6}

according to the rule of mixture. Then,

$$\begin{aligned} E^*(z) &= E_1 + (E_2 - E_1)\hat{V}(z), \\ \nu^*(z) &= \nu_1 + (\nu_2 - \nu_1)\hat{V}(z), \\ \alpha^*(z) &= \alpha_1 + (\alpha_2 - \alpha_1)\hat{V}(z), \end{aligned} \quad (8)$$

where the subscripts 1 and 2 refer to the respective homogeneous material layers (see Fig. 1).

In the majority of practical applications involving functionally graded materials, they are used as interlayers between two homogeneous materials. For such cases, the through-thickness variation of the elastic modulus in the three-layered system is

$$E^*(z) = \begin{cases} E_1 & \text{for } -h_1 \leq z \leq -a, \\ E_1 + \Delta E \hat{V}(z) & \text{for } -a \leq z \leq a, \\ E_2 & \text{for } a \leq z \leq h_2, \end{cases} \quad (9)$$

where $\Delta E = E_2 - E_1$. Similar relations can be obtained for $\nu^*(z)$ and $\alpha^*(z)$.

Substituting Eq. (9) into Eq. (4) leaves the thermo-elastic plane stress solution for an arbitrary FGM characterised by a generic composition profile function $\hat{V}(z)$,

$$\tilde{\sigma}^*(z) = \begin{cases} E_1[\varepsilon_0 + \kappa z - \alpha_1 \Delta T] & \text{for } -h_1 \leq z \leq -a, \\ (E_1 + \Delta E \hat{V}(z))[\varepsilon_0 + \kappa z - (\alpha_1 + \Delta \alpha \hat{V}(z))\Delta T] & \text{for } -a \leq z \leq a, \\ E_2[\varepsilon_0 + \kappa z - \alpha_2 \Delta T] & \text{for } a \leq z \leq h_2. \end{cases} \quad (10)$$

The thermo-elastic solution for the biaxial stress case (i.e., $l = w$ in Fig. 1(a)) can be readily obtained from the plane stress solution by replacing E_i by $E_i/(1 - \nu_i)$ in Eq. (10), for $i = 1, 2$. Furthermore, for plane strain conditions, E_i and α_i in Eq. (10) should be replaced by $E_i/(1 - \nu_i^2)$ and $\alpha_i(1 + \nu_i)$, respectively, for $i = 1, 2$.

2.2. Application to a Ni-FGM- Al_2O_3 system

Consider a system made up of Ni-FGM- Al_2O_3 layers, with all layers assumed to be isotropic elastic materials, free of damage and having the temperature independent properties given in Table 1.

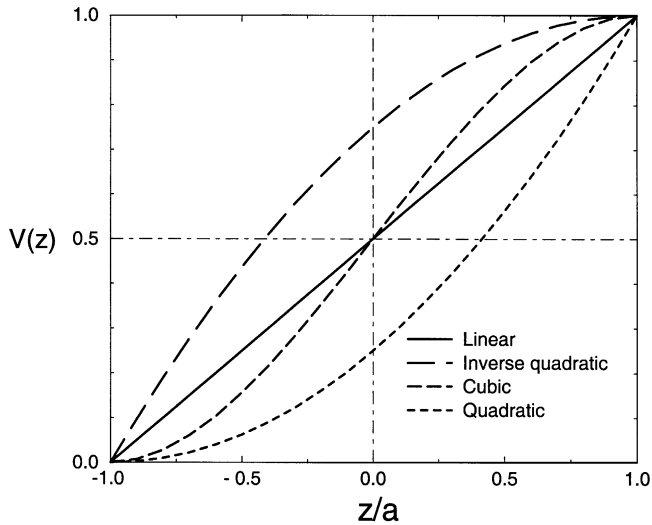


Fig. 2. Different composition profiles used to describe the variation of ceramic volume fraction in the FGM layer.

A thermal history consisting of a temperature drop from a typical processing (e.g. stress free) temperature of 320°C to 20°C is considered. For illustration purposes, the metal and ceramic layer thicknesses will be taken to be one-half that of the FGM layer, viz. $h = h_1 = h_2 = a$. Although plane stress conditions are assumed, solutions to other plane conditions can simply be obtained in the way described in Section 2.1.

The compositional gradation of the FGM layer is defined by the volume fraction of the ceramic phase. Here, the following functions of $\hat{V}(z)$ will be considered:

1. Linear: $\hat{V}(z) = \frac{z+a}{2a},$
 2. Quadratic: $\hat{V}(z) = \left(\frac{z+a}{2a}\right)^2,$
 3. Inverse quadratic: $\hat{V}(z) = 1 - \left(\frac{a-z}{2a}\right)^2,$
 4. Cubic: $\hat{V}(z) = 3\left(\frac{z+a}{2a}\right)^2 - 2\left(\frac{z+a}{2a}\right)^3.$
- (11)

These functions are illustrated in Fig. 2.

To verify the accuracy of the analytical solutions, finite element analyses of the three-layered system were performed using the commercial finite element code ABAQUS (1999). Due to symmetry considerations, only half of the three-layered system was modelled using 1000 equal sized linear plane stress elements. The length-to-height ratio for the model was chosen to be $l/(h_1 + h_2) = 2.5$ so as to minimise edge effects.

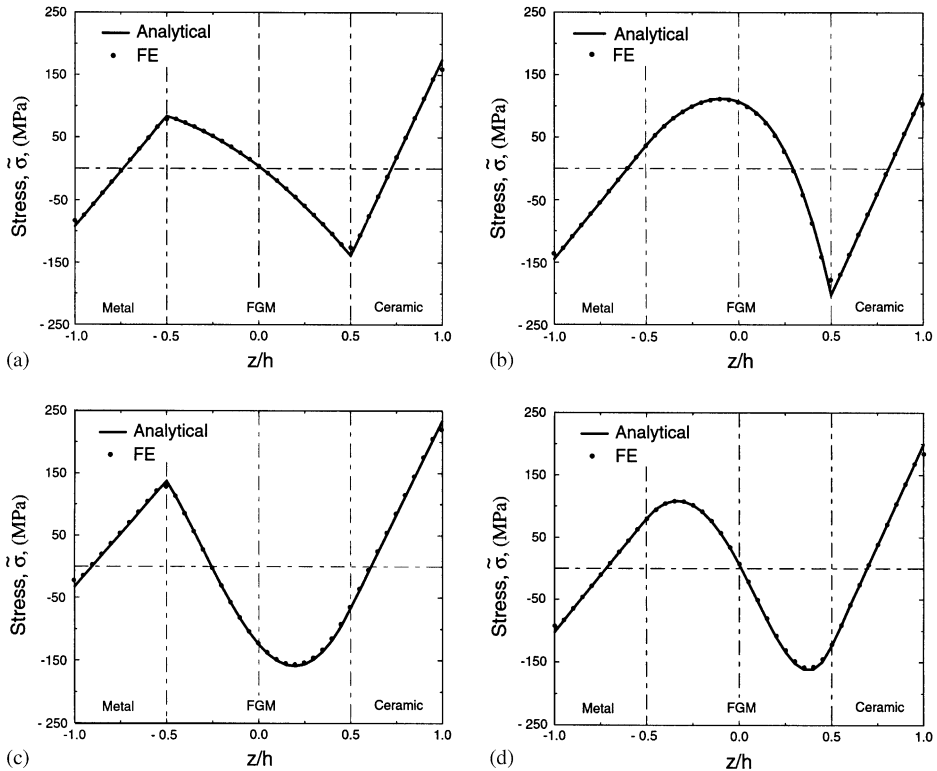


Fig. 3. Analytical thermo-elastic residual stress distributions at room temperature and corresponding FE predictions using an FGM with a (a) linear, (b) quadratic, (c) inverse quadratic and (d) cubic compositional variation ($T_0 = 320^\circ\text{C}$).

The FGM layer was modelled with continuously varying composition and properties through the thickness. To implement that, an implicit user-defined material subroutine was developed and used in the FE calculations.

Figs. 3(a)–(d) show the stress distributions through the thickness of the three-layered system for the different composition profiles at room temperature. The analytical predictions are in good agreement with the FE results. It can be seen that the stress distributions in the homogeneous metallic and ceramic layers are close to being linear and hence consistent with Eq. (10), whereas the stress distribution in the FGM layer depends on the type of compositional gradation. It is also worth noting that the stresses at the ceramic/FGM interface are always compressive whereas those at the metal/FGM interface are tensile in all cases. The reverse is true if the FGM system temperature increases from the stress-free temperature (viz. 320°C). In the linear profile case (Fig. 3(a)), the stress within the FGM varies parabolically and is close to zero at the FGM mid-plane. Peak tensile and compressive stresses are observed at the ceramic surface and the ceramic/FGM interface, respectively. The stresses across the metal/FGM interface for the quadratic gradation (Fig. 3(b)) and across the ceramic/FGM interface

for the inverse quadratic gradation (Fig. 3(c)) are continuous. This is due to the very gradual transition of the FGM composition near those interfaces.

Compared to the linear profile, the quadratic gradation gives a measurably smaller (tensile) stress at the metal/FGM interface at the expense of a higher (compressive) stress at the ceramic/FGM interface. A lower tensile stress is found in the ceramic layer and the peak (tensile) stress develops near the FGM mid-plane. The inverse quadratic gradation reduces the magnitude of the (tensile) stress at the metal surface by 65% from the linear profile case. As can be seen in Fig. 3(d), by using the cubic gradation, the stresses across both interfaces vary smoothly and the interfacial stress magnitudes are comparable to the linear case.

Possible failure mechanisms in the ceramic include cleavage fracture from pre-existing microcracks caused by high tensile stresses. Thus, the inverse quadratic composition profile appears to be the least suitable as it yields the highest tensile stress in the ceramic. In contrast, high triaxialities ($\sigma_m = \tilde{\sigma}/3$) in the metal layer or the metal-rich region of the FGM can lead to ductile failure. Again, the quadratic composition profile exhibits the highest triaxialities. Furthermore, since void growth is mainly affected by the mean triaxial stress, it is therefore more likely to take place in the biaxial stress case than in the plane stress case. Among all composition profiles considered here, the linear and the cubic profiles appear to be the most benign.

3. Thermo-elastoplastic analysis

3.1. Self-consistent constitutive formulation

In this section, the elastoplastic behaviour of the metallic phase within the FGM in the three-layered system illustrated in Fig. 1 is considered. Layer 1 is assumed to be an elastoplastic metal and Layer 2 an elastic ceramic material. Plane stress conditions will be considered as an example. The metal is assumed to have its constitutive behaviour described by a power-law hardening law, namely

$$\tilde{\varepsilon}_1 = \begin{cases} \frac{\tilde{\sigma}_1}{E_1} & \text{if } \tilde{\sigma}_1 \leq \sigma_{y_1}, \\ \varepsilon_{y_1} \left(\frac{\tilde{\sigma}_1}{\sigma_{y_1}} \right)^n & \text{otherwise.} \end{cases} \quad (12)$$

Here σ_{y_1} and ε_{y_1} ($= \sigma_{y_1}/E_1$) are the metal yield stress and strain, respectively, and n is the strain hardening exponent.

The plastic strain rate in the metal is defined through an associated flow rule as

$$\dot{\varepsilon}_1^p = \frac{\dot{\tilde{\sigma}}_1}{\hat{h}(\tilde{\sigma}_1)}, \quad (13)$$

where $\hat{h}(\tilde{\sigma}_1)$ is the plastic hardening modulus of the metallic phase (Phase 1).

The uniaxial equivalent plastic strain rate in the FGM, $\dot{\varepsilon}^{*p}$, is simply given by the volume average of that in the metallic phase, ($\dot{\varepsilon}_1^p$),

$$\dot{\varepsilon}^{*p}(z) = f_1(z)\dot{\varepsilon}_1^p \quad (14)$$

where f_1 denotes the volume fraction of the metallic phase within the FGM. In Eq. (14), the dependency of $\dot{\tilde{\epsilon}}^{*p}$ on the out-of-plane coordinate has been included to account for the spatial variation of the material behaviour.

In an analogous way as in the thermo-elastic case, the total strain in the three-layered system, $\tilde{\epsilon}^*$, is considered to be made up of an elastic ($\tilde{\epsilon}^{*e}$), a plastic ($\tilde{\epsilon}^{*p}$) and a thermal component ($\tilde{\epsilon}^{*th}$), and to depend also on the out-of-plane coordinate (z) (see Fig. 1). The FGM stress rate at a generic location z , $\dot{\tilde{\sigma}}^*$, is given by

$$\dot{\tilde{\sigma}}^*(z) = E^*(z) [\dot{\tilde{\epsilon}}^*(z) - \dot{\tilde{\epsilon}}^{*p}(z) - \dot{\tilde{\epsilon}}^{*th}(z)], \quad (15)$$

where $\dot{\tilde{\epsilon}}^{*th} = \alpha^*(z)\dot{T}$, with \dot{T} being the temperature rate and $E^*(z)$ is the FGM modulus defined in Eq. (9). An expression for $\dot{\tilde{\epsilon}}^*(z)$ can be readily found from the differential form of Eq. (3),

$$\dot{\tilde{\epsilon}}^*(z) = \dot{\epsilon}_0 + \dot{\kappa}z, \quad (16)$$

where $\dot{\epsilon}_0$ and $\dot{\kappa}$ are their differential forms.

The homogenisation of the local elastoplastic properties within the FGM is done using a self-consistent approach. Following the recent work of Cailletaud and Pilvin (1995), Busso (1999) and Busso et al. (2001a, b), the homogenisation of the FGM elastoplastic behaviour for ceramic volume fractions greater than 20% requires that the stress in each individual FGM phase, $\tilde{\sigma}_i$, be related to the macroscopic FGM stress, $\tilde{\sigma}^*$, in terms of interphase accommodation factors for each phase, \tilde{S}_i . Then,

$$\dot{\tilde{\sigma}}_i(z) = \dot{\tilde{\sigma}}^*(z) + 2\mu^*(1 - \beta) \left\{ \left(\sum_{k=1}^m f_k \dot{\tilde{S}}_k \right) - \dot{\tilde{S}}_i \right\}, \quad (17)$$

where μ^* is the FGM shear modulus, β Eshelby's elastic accommodation factor and m the number of elastoplastic phases ($m = 1$ in this case). The evolution of the interphase accommodation variable is given by

$$\dot{\tilde{S}}_i = \dot{\tilde{\epsilon}}_i^p - \hat{H}(f_i) \tilde{S}_i |\dot{\tilde{\epsilon}}_i^p|, \quad (18)$$

where $\hat{H}(f_i)$ is a dimensionless homogenisation function which needs to be calibrated from detailed finite element calculations of the metal–ceramic system, and $|\dot{\tilde{\epsilon}}_i^p|$ is the magnitude of $\dot{\tilde{\epsilon}}_i^p$. The calibration of \hat{H} using an embedded unit cell technique will be described in Section 3.2.

Eqs. (12)–(18) constitute the complete set of constitutive and compatibility relations for the three-layered system. In this work, they were numerically integrated using an Euler forward integration scheme and the results will be shown in Section 3.4. For a general three-dimensional form of the formulation, see Appendix A.

3.2. Calibration of $\hat{H}(f_i)$ using an embedded unit cell finite element approach

An embedded unit cell approach (e.g. Dong and Schmauder, 1996; Forest and Pilvin, 1996) is relied upon to calibrate the function $\hat{H}(f_i)$ (Eq. (18)) so that self-consistency in both strains and stresses is satisfied under uniaxial loading conditions. The FE unit cell model consists of a spherical inclusion, made up of a ceramic core embedded

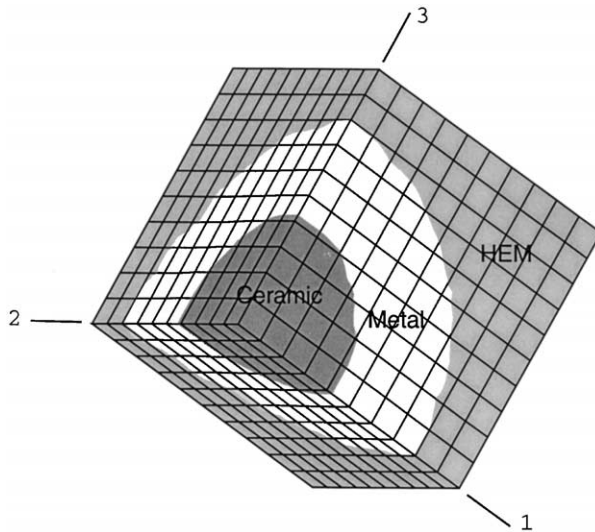


Fig. 4. FE model for the embedded unit cell calculations with $f_2 = 0.4$ consisting of a ceramic–metal inclusion embedded in the HEM matrix. Only one-eighth of the unit cell is shown.

in an outer metallic shell which is, in turn, centred inside a cube of a homogeneous equivalent material (HEM) (see Fig. 4). Note that embedded cell models of this type are known to represent more accurately the behaviour of composites with randomly arranged particles (Dong and Schmauder, 1996).

The behaviour of the HEM is described by the proposed FGM self-consistent constitutive formulation and that of the metal and the ceramic phases within the spherical inclusion by their bulk elastoplastic and elastic properties, respectively. For self-consistency to be satisfied, $\hat{H}(f_i)$ is calibrated so that, for a given ceramic volume fraction, $f_2 (= 1 - f_1)$, the stress–strain response of the HEM matches that of the spherical two-phase inclusion. Due to symmetry considerations, only one-eighth of the model was considered (see Fig. 4). A user-defined material subroutine was developed which allows the material properties at each integration point of the FE model to be identified from its spatial coordinates and the ceramic phase volume fraction. Such approach enables the use of a single relatively regular 3D FE mesh (see Fig. 4) to analyse the response of the embedded unit cell model for a wide range of ceramic volume fractions. A mesh sensitivity study revealed the 3D FE mesh shown in Fig. 7, which consists of 1000 3D quadratic isoparametric elements, to yield mesh-independent results. Symmetry boundary conditions were prescribed on the $X_1 = 0$, $X_2 = 0$ and $X_3 = 0$ planes and periodic boundary conditions on the remaining faces of the unit cell. Uniaxial loading was simulated by imposing appropriate displacement boundary condition along any one of the three orthogonal directions.

The thermo-elastic properties used for the individual Ni and Al_2O_3 phases are those given in Table 1. The Ni yield stress was taken to be temperature-independent and equal to 100 MPa, and its strain hardening exponent, $n = 5$ (Frost and Ashby, 1982).

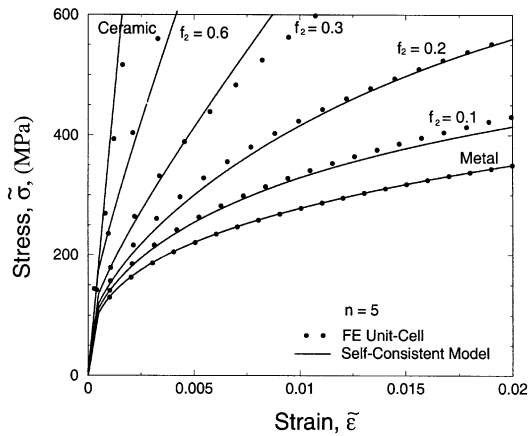


Fig. 5. Comparison between the uniaxial stress–strain response of the ceramic–metal composite calculated with the FE unit cell models and the self-consistent predictions.

Eqs. (13)–(15) and (17)–(18) were numerically integrated using an Euler forward scheme. The dimensionless parameter \hat{H} was calibrated for the range $0 < f_2 < 1$ and the optimum values found to be linearly dependent on the ceramic volume fraction, f_2 ,

$$\hat{H}(f_2) = h_0 + h_1 f_2 \quad \text{for } f_2 \leq 0.4, \quad (19)$$

with $h_0 = 135$ and $h_1 = -340$. If $f_2 > 0.4$, $\hat{H} = 0$.

3.3. Uniaxial response of the Ni–Al₂O₃ composite: a comparison between the proposed self-consistent model and an existing variational formulation

3.3.1. Self-consistent method

The self-consistent formulation derived in Section 3.1 is used together with the calibrated homogenisation function \hat{H} to predict the uniaxial stress–strain response of Ni–Al₂O₃ composites with a range of reinforcement volume fractions. A comparison between the self-consistent predictions of the uniaxial FGM stress–strain response and accurate FE results obtained with the unit cell model is given in Fig. 5. It can be seen that good agreement is generally found for the range of ceramic volume fractions considered, except at $f_2 = 0.3$ where the hardening rate is overpredicted at large strains.

3.3.2. Alternative homogenisation procedure based on a variational principle

The effective behaviour of a nonlinear composite can alternatively be described using a variational approach, such as that proposed by Li and Ponte Castañeda (1994). This method will be briefly summarised next and its predictive capabilities compared with those of the proposed self-consistent approach for the Ni–Al₂O₃ system.

In the variational approach, the constitutive behaviour of nonlinear composite materials relies on an effective stress potential function, $\tilde{U}(\sigma_{ij}^*)$, such that,

$$\varepsilon_{ij}^* = \frac{\partial \tilde{U}(\sigma_{ij}^*)}{\partial \sigma_{ij}^*}, \tag{20}$$

where ε_{ij}^* and σ_{ij}^* represent the average composite strain and stress components, respectively. For isotropic composites with a power-law strain hardening metallic matrix reinforced by elastic particles, the uniaxial stress potential is given by (Li and Ponte Castañeda, 1994),

$$\tilde{U}(\sigma_{ij}^*) = \begin{cases} \frac{\sigma_{11}^{*2}}{2} \hat{d}(\mu_0 = \mu_1) & \text{if } \hat{\Phi}(\sigma_{11}^*) \leq 0, \\ \max \left[\frac{\sigma_{11}^{*2}}{2} \hat{d}(\mu_0) - f_1 \hat{V}(\mu_0) \right] & \text{if } \hat{\Phi}(\sigma_{11}^*) > 0. \end{cases} \tag{21}$$

Here, $\hat{\Phi}(\sigma_{11}^*)$ is the yield function, μ_1 the elastic shear modulus of the metallic phase 1, and μ_0 the shear modulus of the linear elastic comparison composite. The function $\hat{V}(\mu_0)$ is, in turn, given by

$$\hat{V}(\mu_0) = \left(\frac{n-1}{n+1} \right) \frac{\tau_{y1}^2}{2\mu_1} \left[\left(\frac{\mu_1}{\mu_0} \right)^{(n+1)/n-1} - 1 \right], \tag{22}$$

where τ_{y1} and n are the metal yield stress in shear and hardening exponent, respectively. The function $\hat{d}(\mu_0)$ is defined as

$$\hat{d}(\mu_0) = \frac{1}{9k_1} \left[1 + f_2 \frac{\hat{\mu} + f_1(C_s - 2G_s)}{C} \right] + \frac{1}{3\mu_0} \left[1 + f_2 \frac{\hat{k} + f_1(C_s + G_s)}{C} \right], \tag{23}$$

where f_2 is the reinforcement volume fraction and $f_1 = 1 - f_2$, $\hat{k} = k_2/(k_1 - k_2)$ and $\hat{\mu} = \mu_2/(\mu_0 - \mu_2)$. Here k_i and μ_i are the bulk and shear moduli of the phase (i), for $i = 1$ and 2.

The parameters C , C_s , D_s , G_s and H_s are given by

$$\begin{aligned} C &= \hat{k}\hat{\mu} + \frac{f_1}{3}\hat{k}(2D_s + C_s - 2H_s - 2G_s) \\ &+ \frac{f_1}{3}\hat{\mu}(D_s + 2C_s + 2H_s + 2G_s) + f_1^2(C_s D_s - 2G_s H_s), \\ C_s &= 1 - (S_{2222}^{(1)} + S_{2233}^{(1)}), \quad D_s = 1 - S_{1111}^{(1)}, \\ G_s &= -S_{1122}^{(1)}, \quad H_s = -S_{2211}^{(1)}. \end{aligned} \tag{24}$$

Here $S_{ijkl}^{(1)}$ are the components of the Eshelby’s tensor (Eshelby, 1957) associated with phase 1. The yield function, $\hat{\Phi}(\sigma_{11}^*)$, defined so that $\hat{\Phi} < 0$ for elastic deformation,

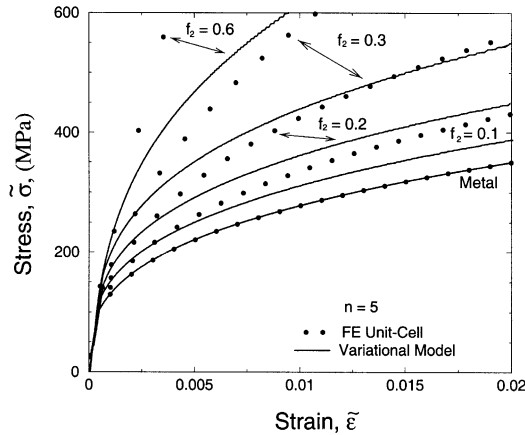


Fig. 6. Comparison between the uniaxial stress–strain response calculated with the FE unit cell models and the variational method predictions.

$\hat{\Phi} = 0$ at yield, and $\hat{\Phi} > 0$ for plastic loading, is given by

$$\hat{\Phi}(\sigma_{11}^*) = - \left[\frac{\sigma_{11}^{*2}}{2} \frac{\partial \hat{d}(\mu_0 = \mu_1)}{\partial \mu_0} + \frac{f_1}{2} \left(\frac{\tau_{y1}}{\mu_1} \right)^2 \right]. \tag{25}$$

Finally, by using Eqs. (20) and (21), the uniaxial stress–strain relation is

$$\sigma_{11}^* = \begin{cases} \varepsilon_{11}^* / \hat{d}(\mu_0 = \mu_1) & \text{if } \hat{\Phi}(\sigma_{11}^*) \leq 0, \\ \varepsilon_{11}^* / \hat{d}(\mu_0 = \tilde{\mu}_0) & \text{if } \hat{\Phi}(\sigma_{11}^*) > 0, \end{cases} \tag{26}$$

where $\tilde{\mu}_0$ is the optimal value of μ_0 obtained from Eq. (21).

In Fig. 6, the uniaxial responses predicted by Eqs. (26) for pure Ni reinforced with different Al_2O_3 volume fractions (i.e. 10%, 20%, 30% and 60%) are presented together with the accurate reference solutions obtained from the FE unit cell analyses. It can be seen that, for this particular composite, the variational model does not predict the elastoplastic behaviour of the composites as accurately as the proposed self-consistent method. This is due to the fact that this type of variational formulation is particularly suited to composite materials with a large elastic property mismatch between its phases. For the Ni– Al_2O_3 composite, the elastic modulus ratio is only 1.8 (see Table 1).

Next, the self-consistent approach will be used to study the thermo-elastoplastic behaviour of the Ni–FGM– Al_2O_3 three-layered system.

3.4. Application to a Ni–FGM– Al_2O_3 system

The stress distributions within the Ni–FGM– Al_2O_3 system using the homogenised constitutive formulation outlined in Section 3.1 were determined for the composition profiles illustrated in Fig. 2. A temperature drop from the stress-free temperature of

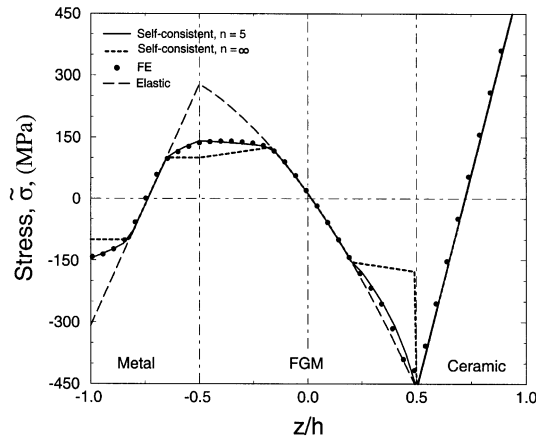


Fig. 7. Comparison between the self-consistent solution and FE results at room temperature for a linear composition profile.

620°C to room temperature is considered as the thermal transient. The cooling rates are assumed to be such that time-dependent effects are negligible.

For comparison, reference solutions were obtained from finite element analyses of the three-layer system with the elastoplastic behaviour of the FGM given by the results from the FE unit cell calculations.

Fig. 7 shows a comparison between the self-consistent predictions and the FE results for the linear composition profile with continuously varying FE properties in the FGM region. The stress distributions corresponding to an elastic, a perfectly plastic ($n = \infty$), and a strain hardening (with $n = 5$) metallic phase are shown. It can be seen that yielding takes place at the metal surface and at both the metal-rich and ceramic-rich ends of the FGM. The magnitude of the peak (tensile) stress in the FGM is reduced by 65% as a result of plasticity in the FGM metallic phase. A sharp inflection in the stress distribution is observed at the ceramic/FGM interface due to the purely elastic behaviour of the ceramic. Note that the locations where plasticity is predicted to occur in Fig. 7 (e.g. at the metal-free surface, the metal/FGM interface and in the ceramic-rich region) generally agree with the FE predictions of Weissenbek et al. (1997), where the ceramic particles within the FGM were explicitly modelled as elastic isotropic materials. However, they found that plastic deformation also occurs in the middle of the graded FGM layer as a result of the local constraint exerted by the ceramic particles.

In Figs. 8–10, both the elastic, and the self-consistent elastoplastic solutions with $n = 5$ are shown together with the FE results for the nonlinear composition profiles. It can be seen that the self-consistent predictions for all the composition profiles agree well with the FE results. In the quadratic profile, Fig. 8, compressive yielding starts from the metal surface and tensile yielding occurs within the FGM. The stresses in both regions show a considerable reduction when compared with the elastic solution. Small yielded regions are also seen in the ceramic-rich side of the FGM. The inverse quadratic

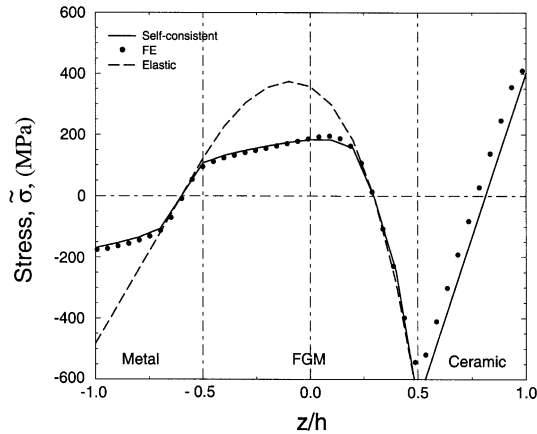


Fig. 8. Comparison between the self-consistent thermal stress distributions with the FE results for a quadratic compositional variation ($n = 5$).

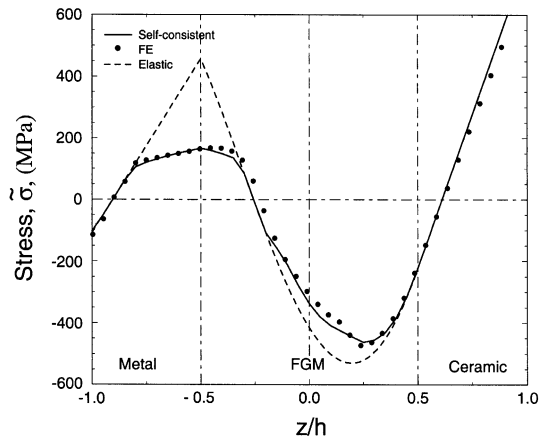


Fig. 9. Comparison between the self-consistent thermal stress distributions with the FE results for an inverse quadratic compositional variation ($n = 5$).

profile (Fig. 9) shows yielding occurring mainly around the metal/FGM interface and within the FGM, with the former region being in tension and the latter in compression. A similar trend can be observed for the cubic profile case (Fig. 10).

As the self-consistent FGM predictions cannot account for the effects of the packing arrangement of the individual ceramic particles within the FGM, it is of interest to investigate their relative accuracy. To that purpose, the uniaxial FE results of Weissenbek et al. (1997) obtained from FE unit cell models with square and hexagonal packings were compared with those obtained with the proposed self-consistent FGM formulation. Fig. 11 shows the average stress–strain response of the three-layered system obtained by loading it along its in-plane direction (i.e. x -axis in Fig. 1) under

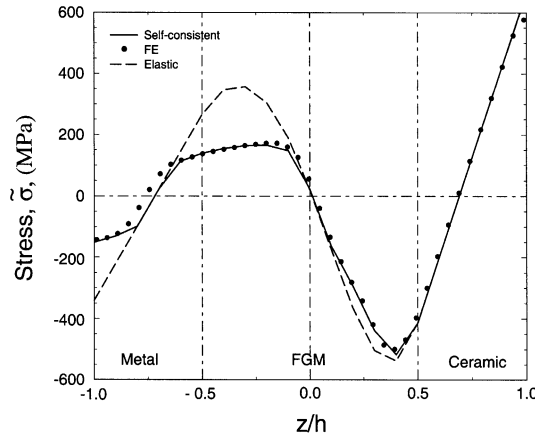


Fig. 10. Comparison between the self-consistent thermal stress distributions with the FE results for a cubic compositional variation ($n = 5$).

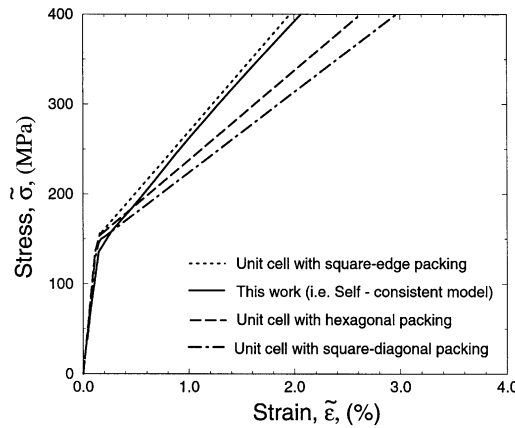


Fig. 11. Comparison between the average in-plane stress–strain response of the three-layered system predicted by the proposed self-consistent model and by the FE results of Weissenbek et al. (1997) based on unit cell computations with square and hexagonal packing of the ceramic particles.

plane stress. The dimensions of the three-layered model were chosen to be identical to those used in Weissenbek et al. (1997). The predicted average in-plane stress–strain response in the three-layered FGM system is shown in Fig. 11, together with the results reported by Weissenbek et al. (1997). It can be seen that the average response given by the self-consistent model lies amongst the periodic unit cell FE results obtained by Weissenbek et al. (1997) with square and hexagonal packing arrangements for the ceramic particles. The overall hardening behaviour increases in the following sequence: square–diagonal packing \rightarrow hexagonal packing \rightarrow self-consistent model \rightarrow square–edge packing. It is encouraging that the overall in-plane system response

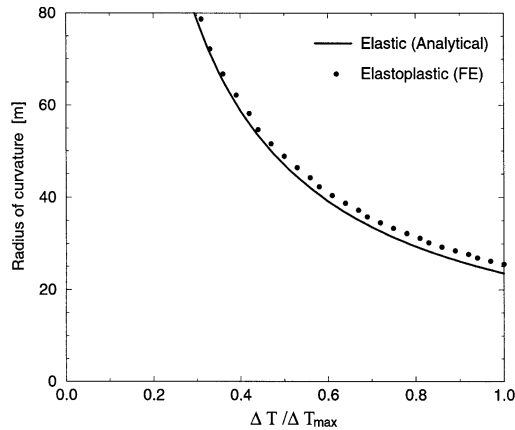


Fig. 12. Radius of curvature of a plane stress three-layered FGM beam undergoing a temperature drop of $\Delta T / \Delta T_{\max}$ from the stress-free temperature assuming elastic and elastoplastic behaviour ($\Delta T_{\max} = 600^{\circ}\text{C}$).

predicted by the self-consistent FGM formulation is well bounded by the periodic unit cell FE results.

A variable which can be generally measured experimentally more easily than the stress distributions is the overall curvature of the FGM system. An analytical solution for the elastic FGM system curvature induced by a temperature change from a curvature-free reference temperature can be found in Freund (1993). However, an elastoplastic curvature needs to be calculated numerically from finite element results. Fig. 12 shows the predicted radius of curvature of a plane stress three-layered FGM beam subjected to different temperature changes ΔT , up to a maximum of $\Delta T_{\max} = 600^{\circ}\text{C}$. Here, the geometry of the FE model was chosen to ensure a uniform curvature throughout the FGM system thickness, and an FGM with an inverse quadratic profile was considered as it shows the most contrasting result. The elastic and elastoplastic predictions shown in Fig. 12 reveal that plasticity only causes the curvature to deviate a relatively small amount from the elastic curvature. This occurs at approximately $\Delta T \approx 0.3\Delta T_{\max}$, which agrees with the onset of plasticity in the FGM metallic phase. It is interesting to note that despite the small differences in the overall curvatures for the elastic and elastoplastic cases, the corresponding rearrangement of the local elastic stresses due to plastic deformation is considerable. For instance, the maximum stress reduction as a result of plastic deformation was found to be as large as 200% (at the metal/FGM interface, see Fig. 9). Therefore, it can be concluded that the curvature alone cannot be used to infer accurately the local elastoplastic stresses within the three-layered FGM system.

If failure is assumed to be controlled by yielding, it is important to determine the critical temperature transient from the stress-free temperature, ΔT_c , that causes the onset of plasticity at either the metal surface or the metal/FGM interface. Fig. 13 shows the critical temperature at which yielding starts at either the metal surface or the metal/FGM interface as a function of the relative FGM thickness, $2a/(h_1 + h_2)$, for the plane stress case and the linear composition profile. These results show that,

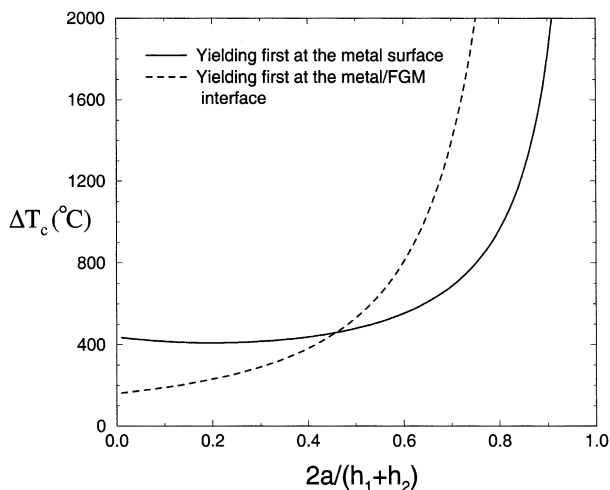


Fig. 13. Critical temperature transient for the onset of plasticity at the metal surface and the metal/FGM interface for the linear FGM compositional variation ($n = 5$).

in a three-layered system of the linear gradation where the FGM layer is relatively thin, yielding will occur first at the metal/FGM interface. The critical relative FGM thickness beyond which yielding switches from occurring first at the interface to the metal surface is approximately $2a/(h_1 + h_2) = 0.46$. This is roughly the same as that of the cubic composition profile. Furthermore, these analyses revealed that, for the quadratic composition profile, yielding also occurs first at the metal/FGM interface and the corresponding critical relative FGM thickness is approximately 0.28. For the case of the inverse quadratic composition profile, yielding always occurs first at the metal/FGM interface regardless of the relative FGM thickness. Based on this type of information, the geometry of the system or/and the FGM composition profile can be chosen so that, for a given temperature transient, yielding at undesirable locations can be avoided.

4. Conclusions

The proposed relations for the thermo-elastic stress distributions within a generic metal–FGM–ceramic system can predict accurately complex stress distributions induced by thermal transients. By choosing an appropriate FGM compositional gradation, the stress distribution within the system can be controlled so that undesirable stresses at critical locations are minimised or avoided. From the choices of the compositional gradation considered here, the linear and the cubic profiles offer the most benign stress distributions.

Elastoplastic solutions for the residual stress distribution in a generic metal–FGM–ceramic system have been proposed and the results agree well with accurate finite element solutions. Two methods were pursued in order to homogenise the FGM elastoplastic

properties, namely a self-consistent method and a variational principle-based approach. The uniaxial response of the Ni–Al₂O₃ composite obtained from both methods were compared with finite element solutions. The self-consistent method was found to predict the composite uniaxial response accurately over a wide range of ceramic volume fractions, whereas the variational formulation, which is better suited to composites with larger elastic property mismatch than what was considered in this work, is relatively less accurate. The stress–strain response of a metal–FGM–ceramic system obtained with the proposed self-consistent method was also in agreement with periodic unit cell FE results reported in the literature.

Predictions of the critical temperature transients from the stress-free temperature that causes yielding at either the metal surface or at the metal/FGM interface have also been obtained. The analytical elastic and semi-analytical self-consistent elastoplastic solutions presented here provide a simple, yet accurate tool for the prediction of thermally induced stresses in an FGM layer sandwiched between two homogeneous materials.

Acknowledgements

Support for this work has been provided by the Government of Thailand. The authors are also very grateful to Prof. Pedro Ponte Castañeda, University of Pennsylvania, USA, for his comments on the discussion of the variational approach. The ABAQUS was provided under academic license by HKS Inc., Providence, Rhode Island, USA.

Appendix A. 3-D generalisation of the self-consistent thermo-elastoplastic constitutive formulation

The FGM uniaxial equivalent stress–strain relations expressed in terms of the out-of-plane coordinate z , see Eq. (15), can be generalised into the following three-dimensional form:

$$\begin{aligned} \dot{\sigma}_{ij}^*(z) = & 2\mu^*(z)\{\dot{\varepsilon}_{ij}^*(z) - \dot{\varepsilon}_{ij}^{*P}(z)\} + \delta_{ij}\lambda^*(z)\{\dot{\varepsilon}_{kk}^*(z) - \dot{\varepsilon}_{kk}^{*P}(z)\} \\ & - \delta_{ij}\{2\mu^*(z) + 3\lambda^*(z)\}\alpha^*(z)\dot{T}, \quad i, j, k = 1, 2, 3, \end{aligned} \quad (\text{A.1})$$

where $\dot{\varepsilon}_{ij}^*$ is the total strain rate component due to the temperature-induced local curvature change (e.g., see Eq. (16)), $\dot{\varepsilon}_{ij}^{*P}$ the overall plastic strain rate component, μ^* , λ^* and α^* are the FGM shear modulus, Lamé constant, and coefficient of thermal expansion, respectively, δ_{ij} the Kronecker delta and \dot{T} the temperature rate. The spatial variations of μ^* , λ^* and α^* in the FGM are given by Eq. (8).

The FGM plastic strain rate is defined by

$$\dot{\varepsilon}_{ij}^{*P} = f_1 \dot{\varepsilon}_{1,ij}^P, \quad (\text{A.2})$$

where f_1 is the volume fraction of the metallic phase and $\dot{\epsilon}_{1ij}^p$ its plastic strain rate given by

$$\dot{\epsilon}_{1ij}^p = \langle \dot{\chi}_1 \rangle \frac{\sigma'_{1ij}}{\sigma_{e1}}. \quad (\text{A.3})$$

Here σ'_{1ij} is the deviatoric stress component of the metallic phase, σ_{e1} the equivalent stress,

$$\sigma_{e1} = \left(\frac{3}{2} \sigma'_{1ij} \sigma'_{1ij} \right)^{1/2} \quad (\text{A.4})$$

and $\langle \dot{\chi}_1 \rangle$ a switching parameter so that

$$\langle \dot{\chi}_1 \rangle = \begin{cases} \frac{3}{2} \frac{\dot{\sigma}_{e1}}{h} & \text{if } \sigma_{e1} \geq \sigma_{y1} \quad \text{while loading,} \\ 0 & \text{if } \sigma_{e1} < \sigma_{y1} \quad \text{or } \sigma_{e1} = \sigma_{y1} \quad \text{while unloading,} \end{cases} \quad (\text{A.5})$$

where $h = \hat{h}(\sigma_{e1})$ is the plastic hardening modulus of the metallic phase, and σ_{y1} the metal yield stress.

The stress within a generic elastoplastic FGM phase, r , can be expressed in terms of the corresponding interphase accommodation factor, S_{rij} , as,

$$\dot{\sigma}_{rij} = \dot{\sigma}_{ij}^* + 2\mu^*(1 - \beta) \left\{ \sum_{k=1}^m f_k \dot{S}_{kij} - \dot{S}_{rij} \right\}, \quad (\text{A.6})$$

where β is Eshelby's elastic accommodation factor and m the number of elastoplastic phases ($=1$ in the Ni–Al₂O₃ system considered here). The evolution of S_{rij} is given by

$$\dot{S}_{rij} = \dot{\epsilon}_{rij}^p - \hat{H}(f_r) S_{rij} |\dot{\epsilon}_{rij}^p|, \quad (\text{A.7})$$

where $\hat{H}(f_r)$ is the dimensionless homogenisation function.

References

- ABAQUS, 1999. Version 5.8. HKS Inc., Providence, RI, USA.
- Berveiller, B., Zaoui, A., 1979. An extension of the self-consistent scheme to plastically flowing polycrystals. *J. Mech. Phys. Solids* 26, 325–344.
- Budiansky, B., Wu, T.Y., 1962. Theoretical prediction of plastic strains of polycrystals. *Proceedings of the Fourth U.S. National Congress of Applied Mechanics*, p. 1175.
- Busso, E.P., 1999. Oxidation-induced stresses in ceramic–metal interfaces. *J. Phys. IV* 9, 287–296.
- Busso, E.P., Lin, J., Sakurai, S., Nakayama, M., 2001a. A mechanistic study of oxidation-induced degradation in a plasma-sprayed thermal barrier coating system. Part I: model formulation. *Acta Mater.* 49/9, 1515–1528.
- Busso, E.P., Lin, J., Sakurai, S., 2001b. A mechanistic study of oxidation-induced degradation in a plasma-sprayed thermal barrier coating system. Part II: life prediction model. *Acta Mater.* 49/9, 1529–1536.
- Cailletaud, G., Pilvin, P., 1995. *Rev. Eur. Eléments Finis* 3, 515–541.

- Choules, B., Kokini, K., 1996. Architecture of functionally graded ceramic coatings against surface thermal fracture. *J. Eng. Mater. Technol. Trans. ASME* 118, 522–528.
- Dao, M., Gu, P., Maewal, A., Asaro, R., 1997. A micromechanical study of residual stresses in functionally graded materials. *Acta Mater.* 45 (8), 3265–3276.
- Dong, M., Schmauder, S., 1996. Modeling of metal matrix composites by a self-consistent embedded cell model. *Acta Mater.* 44 (6), 2465–2478.
- Erdogan, F., 1995. Fracture mechanics of functionally graded materials. *MRS Bull.* 43–44.
- Eshelby, J.D., 1957. The determination of the elastic field of an ellipsoidal inclusion and related problems. *Proc. Royal Soc. London A* 241, 398.
- Finot, M., Suresh, S., 1996. Small and large deformation of thick and thin film multi-layers: effects of layer geometry, plasticity and compositional gradients. *J. Mech. Phys. Solids* 44 (5), 683–721.
- Forest, S., Pilvin, P., 1996. Modelling the cyclic behaviour of two-phase single crystal nickel-base superalloys. In: Pineau, A., Zaoui, A. (Eds.), *IUTAM Symposium on Micromechanics of Plasticity and Damage of Multiphase Materials 1996*. Kluwer Academic Publishers, Dordrecht, pp. 51–58.
- Freund, L.B., 1993. Stress distribution and curvature of a general compositionally graded semiconductor layer. *J. Crystal Growth* 132 (1–2), 341–344.
- Frost, H.J., Ashby, M.F., 1982. *Deformation-Mechanism Maps*. Pergamon Press, Oxford.
- Giannakopoulos, A.E., Suresh, S., Finot, M., Olsson, M., 1995. Elastoplastic analysis of thermal cycling: layered materials with compositional gradients. *Acta Metall. Mater.* 43 (4), 1335–1354.
- Hashin, Z., Shtrikman, S., 1963. A variation approach to the theory of the elastic behaviour of multiphase materials. *J. Mech. Phys. Solids* 11, 127–140.
- Howard, S.J., Tsui, Y.C., Clyne, T.W., 1994a. The effect of residual stresses on the debonding of coatings—I: a model for delamination at a bimaterial interface. *Acta Metall. Mater.* 42 (8), 2823–2836.
- Howard, S.J., Tsui, Y.C., Clyne, T.W., 1994b. The effect of residual stresses on the debonding of coatings—II: an experiment study of a thermally sprayed system. *Acta Metall. Mater.* 42 (8), 2837–2844.
- Jin, Z.H., Batra, R.C., 1996. Some basic fracture mechanics concepts in functionally graded materials. *J. Mech. Phys. Solids* 44 (8), 1221–1235.
- Kroner, E., 1961. Zur plastischen verformung des vielkristalls. *Acta Metall. Mater.* 9, 153.
- Lee, Y.D., Erdogan, F., 1994/1995. Residual/thermal stresses in FGM and laminated thermal barrier coatings. *Int. J. Fract.* 69, 145–165.
- Li, G., Ponte Castañeda, P., 1994. Variational estimates for the elastoplastic response of particle-reinforced metal–matrix composites. *Appl. Mech. Rev.* 47 (1), S77–94.
- Miyamoto, Y., 1996. The applications of functionally graded materials in Japan—from structure to functional uses. *Mater. Technol.* 11 (6), 230–236.
- Olsson, M., Giannakopoulos, A.E., Suresh, S., 1995. Elastoplastic analysis of thermal cycling: ceramic particles in a metallic matrix. *J. Mech. Phys. Solids* 43 (10), 1639–1671.
- Ponte Castañeda, P., 1991. The effective mechanical properties of nonlinear isotropic composites. *J. Mech. Phys. Solids* 39 (1), 45–71.
- Shaw, L.L., 1998. The crack driving force of functionally graded materials. *J. Mater. Sci. Lett.* 17, 65–67.
- Talbot, D.R.S., Willis, J.R., 1985. Variational principles for inhomogeneous nonlinear media. *IMA J. Appl. Math.* 35, 39–54.
- Weissenbek, E., Pettermann, H.E., Suresh, S., 1997. Elasto-plastic deformation of compositionally graded metal–ceramic composites. *Acta Mater.* 45 (8), 3401–3417.
- Wetherhold, R.C., Seelman, S., Wang, J., 1996. The use of functionally graded materials to eliminate or control thermal deformation. *Compos. Sci. Technol.* 56, 1099–1104.
- Yang, Y.Y., Munz, D., 1997. Stress analysis in a two-materials joint with a functionally graded material. In: Shiota, I., Miyamoto, Y. (Eds.), *Functionally Graded Materials 1996*. Elsevier Science BV, Amsterdam, pp. 41–46.